OFF-PRINTS FROM
MODERN PROBLEMS IN ELASTIC WAVE
PROPAGATION
By Janus Miklowitz and Jan D. Achenbach
Published by John Wiley & Sons, Inc.

MODELING EARTHQUAKES WITH GENERALIZED RAY THEORY

DONALD V. HELMBERGER and DAVID G. HARKRIDER
Division of Geological and Planetary Sciences
California Institute of Technology, Pasadena, CA

ABSTRACT

The complete linear response of plane, elastic layered solid to a shear dislocation is investigated. The solution is expressed as a summation of generalized rays of the P, SV, and SH potentials. This allows the transient response to be obtained upon application of the Cagniard-deHoop technique. Numerical results of the full solution containing the near and far field terms are compared for a whole space, half space, and layered model with asymptotic solutions to establish the advantages and limitations of approximate methods.

INTRODUCTION

In the past decade, significant progress in our understanding of seismograms has been accomplished based largely on our ability to separate source effects from propagational distortions. Numerous formalisms have been developed whereby synthetic seismograms can be computed at various positions on the Earth, for comparisons with observed seismograms. Iterative techniques can then be applied to determine Earth structure or source models or perhaps some properties of both. The most efficient technique used to generate synthetics is essentially controlled by the ratio of the travel time of the disturbance to the source duration, with optics at the upper limit and statics at the lower. However, a highly desirable property of any technique is that the physics be relatively apparent so that the user can easily discern how model parameters influence the synthetic motion. In this paper we will discuss such a technique, called generalized ray theory, where various useful approximations are made based on the travel time to duration ratio.

DIVISION OF GEOLOGICAL SCIENCES
CONTRIBUTION NO.
2959

We assume that earthquakes can be simulated by distributed shear dislocations and that the Earth can be replaced by a layered elastic medium; both assumptions are suspect but worth consideration as viable models at our present level of understanding.

First, we will consider a shear dislocation in a whole space expressed in cylindrical coordinates because of its compatibility with the layered problem. The layered structure complication is effectively removed by a generalized ray expansion of the P, SV, and SH displacement potentials with the Cagniard-deHoop technique used to obtain the transient response. This basic technique has been used earlier by Pekeris [1] and his colleagues, and is sometimes called the Cagniard-Pekeris method by Ben-Menahem and Vered [2]. Japanese seismologists use a similar technique and call it the Cagniard-deHoop-Sato method (Kawasaki et al. [3]). The basic idea appears to have originated with Lamb [4] and has been modified for special purposes by many researchers.

SHEAR DISLOCATION SOURCE

Haskell [5] introduced a shear fault where a discontinuity in displacement across a fault plane was allowed, resulting in a double-couple radiation pattern. Following deHoop's [6] form of the elastodynamic representation, Harkrider [7] has obtained convenient forms of displacements and displacement potentials for a number of different coordinate systems. The solution in cylindrical coordinates has been further reduced to a form suitable for the application of Cagniard's method by Helmberger [8] and Langston and Helmberger [9]. The results in terms of the Laplaced transformed displacements along the vertical, tangential, and radial directions are:

$$\hat{W} = \frac{\partial \hat{\phi}}{\partial z} + sp\hat{\Omega}$$

$$\hat{V} = \frac{1}{r}\frac{\partial \hat{\phi}}{\partial \theta} - \frac{1}{spr}\frac{\partial^2 \hat{\Omega}}{\partial z \partial \theta} - \frac{\partial \hat{\chi}}{\partial r} \qquad (1)$$

$$\hat{Q} = \frac{\partial \hat{\phi}}{\partial r} - \frac{1}{sp}\frac{\partial^2 \hat{\Omega}}{\partial r \partial z} + \frac{1}{r}\frac{\partial \hat{\chi}}{\partial \theta}$$

where z, r, and θ are the vertical, radial and polar angle coordinates, respectively. The P wave potential (ϕ), the SV wave potential (Ω), and the SH wave potential (χ) are expressed by:

P-wave:

$$\hat{\phi} = + \frac{M_o}{4\pi\rho} \frac{2}{\pi} \operatorname{Im} \int_c^{+i\infty+c} C_1(p) \frac{p}{\eta_\alpha} \exp(-s\eta_\alpha|z-h|)K_2(spr)dp \cdot A_1(\theta,\lambda,\delta)$$

$$+ \frac{M_o}{4\pi\rho} \frac{2}{\pi} \operatorname{Im} \int_c^{+i\infty+c} C_2(p) \frac{p}{\eta_\alpha} \exp(-s\eta_\alpha|z-h|)K_1(spr)dp \cdot A_2(\theta,\lambda,\delta)$$

$$+ \frac{M_o}{4\pi\rho} \frac{2}{\pi} \operatorname{Im} \int_c^{+i\infty+c} +C_3(p) \frac{p}{\eta_\alpha} \exp(-s\eta_\alpha|z-h|)K_o(spr)dp \cdot A_3(\theta,\lambda,\delta).$$

SV-waves:

$$\hat{\Omega} = + \frac{M_o}{4\pi\rho} \frac{2}{\pi} \operatorname{Im} \int_c^{+i\infty+c} SV_1(p) \frac{p}{\eta_\beta} \exp(-s\eta_\beta|z-h|)K_2(spr)dp \cdot A_1(\theta,\lambda,\delta)$$

$$+ \frac{M_o}{4\pi\rho} \frac{2}{\pi} \operatorname{Im} \int_c^{+i\infty+c} SV_2(p) \frac{p}{\eta_\beta} \exp(-s\eta_\beta|z-h|)K_1(spr)dp \cdot A_2$$

$$+ \frac{M_o}{4\pi\rho} \frac{2}{\pi} \operatorname{Im} \int_c^{+i\infty+c} SV_3(p) \frac{p}{\eta_\beta} \exp(-s\eta_\beta|z-h|)K_o(spr)dp \cdot A_3 .$$

SH-waves:

$$\hat{\chi} = + \frac{M_o}{4\pi\rho} \frac{2}{\pi} \operatorname{Im} \int_c^{+i\infty+c} SH_1(p) \frac{p}{\eta_\beta} \exp(-s\eta_\beta|z-h|)K_2(spr)dp \cdot A_4$$

$$+ \frac{M_o}{4\pi\rho} \frac{2}{\pi} \operatorname{Im} \int_c^{+i\infty+c} SH_2(p) \frac{p}{\eta_\beta} \exp(-s\eta_\beta|z-h|)K_1(spr)dp \cdot A_5$$

where only the first term of each potential is required in describing a pure strike-slip and the second term only for a pure dip-slip orientation (Harkrider [7]). The more important definitions are as follows:

s = Laplace transform variable

p = ray parameter

$\eta_v = (\frac{1}{v^2} - p^2)^{1/2}$

h = depth of source

α = compressional velocity

β = shear velocity

ρ = density

M_o = seismic moment

with the orientation constants given by:

$$A_1(\theta,\lambda,\delta) = \sin 2\theta \cos\lambda \sin\delta + \frac{1}{2}\cos 2\theta \sin\lambda \sin 2\delta$$

$$A_2(\theta,\lambda,\delta) = \cos\theta \cos\lambda \cos\delta - \sin\theta \sin\lambda \cos 2\delta$$

$$A_3(\theta,\lambda,\delta) = \frac{1}{2}\sin\lambda \sin 2\delta$$

$$A_4(\theta,\lambda,\delta) = \cos 2\theta \cos\lambda \sin\delta - \frac{1}{2}\sin 2\theta \sin\lambda \sin 2\delta$$

$$A_5(\theta,\lambda,\delta) = -\sin\theta \cos\lambda \cos\delta - \cos\theta \sin\lambda \cos 2\delta$$

where

θ = strike from the end of the fault plane

λ = rake angle

δ = dip angle

The vertical radiation patterns, as will become apparent shortly, are defined by

$$C_1 = -p^2 \qquad SV_1 = -\varepsilon p \eta_\beta \qquad SH_1 = \frac{1}{\beta^2}$$

$$C_2 = 2\varepsilon p \eta_\alpha \qquad SV_2 = (\eta_\beta^2 - p^2) \qquad SH_2 = -\frac{\varepsilon}{\beta^2}\frac{\eta_\beta}{p} \qquad (4)$$

$$C_3 = (p^2 - 2\eta_\alpha^2) \qquad SV_3 = 3\varepsilon p \eta_\beta$$

where $\varepsilon = \begin{cases} +1 & z > h \\ -1 & z < h \end{cases}$.

The integrals expressed in (2) can be transformed back into the time domain by the application of the Cagniard-deHoop technique, see Gilbert and Helmberger [10] and Harkrider and Helmberger [11]. For example, the field function defined by

$$\bar{\zeta}_n(r,z,s) = \frac{2}{\pi} s \, \mathrm{Im} \int_c^{i\infty+c} \frac{p}{\eta_v} K_n(spr) \, e^{-s\eta_v|z-h|} \, dp \tag{5}$$

becomes

$$\zeta_n(r,z,t) = \frac{2}{\pi} \frac{\partial}{\partial t} \mathrm{Im} \int_0^t \frac{c_n(t,\tau)}{(t-\tau)^{1/2} \, (t-\tau+2pr)^{1/2}} \left(\frac{dp}{d\tau}\right) \frac{p(\tau)}{\eta_v} \, d\tau, \tag{6}$$

where

$$c_n(t,\tau(p)) = \cosh\left(n \, \cosh^{-1}\left(\frac{t-\tau+pr}{pr}\right)\right) \quad .$$

The geometry is given in Figure 1a and the deHoop contour Γ in Figure 1b, see deHoop [12]. The various functions of p are to be evaluated along Γ defined by choosing those values of p which make $\tau(p)$ real and increasing, where

$$\tau(p) = pr + \eta_v|z-h| \quad . \tag{7}$$

Thus,

$$p(\tau) = \frac{r}{R^2} + i\left(\tau^2 - \frac{R^2}{V^2}\right)^{1/2} |z-h| \tag{8}$$

and

$$\eta(\tau) = \frac{|z-h|\tau}{R^2} - i\left(\tau^2 - \frac{R^2}{V^2}\right)^{1/2} \frac{r}{R^2} \tag{9}$$

and

$$\frac{dp(\tau)}{d\tau} = \frac{i\eta_v(\tau)}{(\tau^2 - R^2/V^2)^{1/2}} \tag{10}$$

where

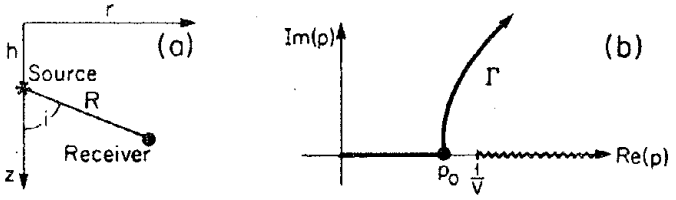

FIGURE 1. Source-Receiver Geometry and Complex (p) Plane with Branch Cut Starting at (1/V) and Running Out along the Real (p) Axes

$$R^2 = r^2 + |z-h|^2 \quad .$$

Note that the integrand is real until

$$p = p_o = \frac{r}{RV} = \frac{\sin i}{V}$$

which is the ray parameter corresponding to Snell's law.

In this simple case we have a closed form solution for various values of η since the equivalent form back in the (ω,k) domain has been evaluated by Harkrider [7]. For example,

$$\zeta_2(r,z,t) = \frac{d}{dt}\left\{\left[\frac{1}{R} + \frac{2V}{r^2}\left(t - \frac{R}{V}\right)\right] H\left(t - \frac{R}{V}\right)\right\} \tag{11}$$

where the near-field contribution appears in terms of r. However, since we need to evaluate integrals similar to (2) with complicated complex integrands later, it should be noted that (6) can be evaluated for various values of (t) after a change of variable as proposed by Helmberger [13]. A relatively fast evaluation of this type of integral is by nonuniform quadrature techniques where the point spacing is determined by the rate of change of the integrand. The accuracy of such techniques will be discussed later. First we will examine some useful approximations by expanding the integrand of (6) in terms of $(t-\tau)^{-1/2}$. Note that

$$c_n(t,\tau,p) = \frac{1}{2}\left[\frac{\left(y+(y^2-1)^{1/2}\right)^{2n} + 1}{\left(y+(y^2-1)^{1/2}\right)^{n}}\right]$$

where

$$y = \frac{t-\tau+pr}{pr}$$

and

$$\frac{c_n(t,\tau,p)}{(t-\tau+2pr)^{1/2}} \simeq \frac{1}{\sqrt{2pr}}$$

to first order. Thus, we can approximate (6) by

$$\zeta_n(v,z,t) = \frac{2}{\pi}\frac{\partial}{\partial t}\,\mathrm{Im}\int_0^t \frac{1}{\sqrt{2pr}}\,\frac{1}{(t-\tau)^{1/2}}\,\frac{dp}{dt}\,\frac{p}{\eta_v}\,d\tau$$

$$= \frac{d}{dt}\left[\frac{1}{\sqrt{t}} * \mathrm{Im}\left(\sqrt{\frac{2}{r}}\,\frac{1}{\pi}\,\frac{\sqrt{p}}{\eta v}\,\frac{dp}{dt}\right)\right] \tag{12}$$

when treating a high frequency source with duration, T, such that $T << 2pr$.

A still further approximation can be used at very large r's when

$$\frac{dp}{dt} = i(t-t_R)^{-1/2} \frac{\eta_v}{(2t_R)^{1/2}}$$

where $t_R = R/V$ and $p = p_o$, and (12) reduces to

$$\zeta_n(r,z,t) = \frac{\delta(t-t_R)}{R} \quad , \tag{13}$$

called the first motion approximation. This approximation is valid at teleseismic distances where the ratio of travel time to duration is of the order of 100 or greater, and has proven quite useful in modeling shallow earthquakes, see Langston and Helmberger [9].

The approximation used in (12) can be obtained in a slightly simpler way by returning to expression (5) and using the asymptotic form of the modified Bessel function, namely

$$K_n(spr) = \sqrt{\frac{\pi}{2spr}}\, e^{-spr} \left[1 + \frac{\mu - 1}{8spr} + \cdots\right]$$

where $\mu = 4n^2$. Substitution of the first term of the above expression into (5) yields (12) after applying the deHoop [12] technique. Note that the second order term has the form of a temporal integration of the first term or the form of a near-field effect. We will discuss the high frequency solution in the next section keeping only the first term; however, the further expansion in higher order terms can be carried out in similar fashion and will be discussed in the numerical results.

HIGH FREQUENCY SOLUTION FOR A MULTILAYER PROBLEM

Applying the method of generalized reflection and transmission coefficients (Spencer [14]), it is possible to construct a representation for a disturbance which has traversed some layering in some specified mode of propagation. The tangential displacement on the surface of a layered half-space model, where only the far-field term is retained, becomes

$$V(r,0,\theta,t) = \frac{M_o}{4\pi\rho_o} \frac{d}{dt} \left[\dot{D}(t) * \sum_{j=1}^{2} A_{j+3}(\theta,\lambda,\delta) V_j(t)\right] \tag{14}$$

where

$$V_j(t) = \frac{2}{r}\frac{1}{\pi}\frac{1}{\sqrt{t}} * \mathrm{Im}\left[\left(\sum_{i=1}^{n}\frac{\sqrt{p}}{\eta_\beta}\,SH_j(p)\;\Pi(p)(p)\;\frac{dp}{dt}\right)_i\right]$$

$\dot{D}(t)$ = far field time history

$\Pi_i(p)$ = product of reflection and transmission coefficients

and the summation is over contributing rays. Numerical evaluation of these expressions are discussed in detail by Helmberber and Malone [15].

The high frequency approximations for the other components of motion are somewhat more complicated with the vertical displacement on the free surface given by

$$W(r,0,\theta,t) = \frac{M_o}{4\pi\rho_o}\frac{d}{dt}\left[\dot{D}(t) * \sum_{j=1}^{3} A_j W_j\right] \tag{15}$$

where

$$W_j(t) = \sqrt{\frac{2}{r}}\frac{1}{\pi}\left[\frac{1}{\sqrt{t}} * \sum_{i=1}^{n}\left(\mathrm{Im}\,\frac{\sqrt{p}}{\eta_\alpha}\,C_j(p)\;R_{NZ}(p)\;\Pi_i(p)\;\frac{dp}{dt}\right)_i\right]$$

$$+ \sqrt{\frac{2}{r}}\frac{1}{\pi}\left[\frac{1}{\sqrt{t}} * \sum_{i=1}^{n}\mathrm{Im}\left(\frac{\sqrt{p}}{\eta_\beta}\,SV_j(p)\;R_{NZ}(p)\Pi_i(p)\;\frac{dp}{dt}\right)_i\right] .$$

The function $\Pi_i(p)$ defines the product of all transmission and reflection coefficients along the path from the source to the receiver. The function $R_{NZ}(p)$ is defined by $R_{PZ}(p)$ or $R_{SZ}(p)$, depending on the mode of propagation upon arrival at the receiver, with

$$R_{PZ} \equiv \frac{2\eta_\alpha(\eta_\beta^2 - p^2)}{\beta^2 R(p)}$$

$$R_{SZ} \equiv \frac{4p\eta_\alpha\eta_\beta}{\beta^2 R(p)} \tag{16}$$

$$R(p) \equiv (\eta_\beta^2 - p^2)^2 + 4p^2\eta_\alpha\eta_\beta \tag{17}$$

R_{PZ} and R_{SZ} are called receiver functions and are derived by taking the limiting conditions as direct P, reflected PP, and SP converge in time at a free surface, see Knopoff et al. [16] and Helmberger [8].

The radial displacement, Q, is obtained by replacing R_{PZ} and R_{SZ} by R_{PR} and R_{SR} defined by

$$R_{PR} = \frac{-4\eta_\alpha \eta_\beta p}{\beta^2 R(p)}$$

$$R_{SR} = \frac{2\eta_\beta (\eta_\beta^2 - p^2)}{\beta^2 R(p)} \qquad (18)$$

The reflection and transmission coefficients used in $\Pi_1(p)$ are those defined by Helmberger [13]. Synthetic responses for these solutions will be discussed after we examine the full Cagniard solution.

FULL CAGNIARD SOLUTION

The high frequency solution discussed in the last section has many advantages in model studies due to its simplicity. However, for small values of (spr), one must use the full solution by applying the transformations used in deriving expression (6). The displacements given by (1) can be evaluated by substituting the potentials (2) and inverting the various terms back into the time domain. The vertical displacement becomes

$$W(r,z,\theta,t) = \frac{M_o}{4\pi\rho_o} \frac{d}{\partial t} \dot{D}(t) * \sum A_j W_j \qquad (19)$$

where W_1, W_2, and W_3 correspond to a pure strike-slip, dip-slip, and 45° dip-slip, respectively. The strike-slip response can be written

$$W_1(r,z,\theta,t) = \frac{2}{\pi} \mathrm{Im} \int^t g_\alpha(2)\ C_1 R_{PZ}\ d\tau$$

$$+ \frac{2}{\pi} \mathrm{Im} \int^t g_\beta(2)\ SV_1 R_{SZ}\ d\tau \qquad (20)$$

where

$$g_v(n) \equiv C(t,\tau,n)\,\frac{p}{\eta_v}\left(\frac{dp}{dt}\right)\,(t-\tau+2pr)^{-1/2}\,(t-\tau)^{-1/2}$$

and

$$R_{PZ} = \eta_\alpha \quad , \qquad R_{SZ} = p \qquad \text{for a whole space} \quad .$$

They are given by expression (16) for a receiver on the free surface. Similar expressions are obtained for the dip-slip and 45° dip-slip cases with n = 1 and n = 0, respectively.

The tangential displacement is slightly more complicated because of the explicit near-field terms

$$V(r,z,\theta,t) = \frac{M_o}{4\pi\rho_o}\frac{d}{dt}\left[\dot{D}(t) * \sum_{j=1}^{2} A_{j+3}\,V_j\right] \tag{21}$$

$$\begin{aligned} V_1(r,z,\theta,t) = {} & \frac{2}{\pi}\,\mathrm{Im}\int^t g_\beta(2)\;SH_1R_T\,d\tau \\ & + \frac{2}{\pi}\,\mathrm{Im}\iint^t g_\beta(2)\;SH_1R_T\left(\frac{2}{pr}\right)\,d\tau\,dt \\ & + \frac{2}{\pi}\,\mathrm{Im}\iint^t g_\alpha(2)\;C_1R_{PT}\left(\frac{2}{r}\right)\,d\tau\,dt \\ & + \frac{2}{\pi}\,\mathrm{Im}\iint^t g_\beta(2)\;SV_1R_{ST}\left(\frac{2}{r}\right)\,d\tau\,dt \end{aligned} \tag{22}$$

where

$$R_T = p, \quad R_{PT} = 1, \quad R_{ST} = -\eta_\beta/p \quad \text{for whole space}$$

and

$$R_T = 2p, \quad R_{PT} = \frac{4\eta_\alpha\eta_\beta}{\beta^2R(p)}, \quad R_{ST} = \frac{-2\eta_\beta}{p}\,\frac{(\eta_\beta^2-p^2)}{\beta^2R(p)}$$

for a receiver on the free surface. The dip-slip result is similar with n = 1 and where the factor in parentheses is reduced by two.

Finally, the most complicated radial component is expressed by

$$Q(r,z,\theta,t) = \frac{M_o}{4\pi\rho_o}\,\frac{d}{dt}\left[\dot{D}(t) * \sum_{j=1}^{3} A_jQ_j\right] \tag{23}$$

where

$$Q_1(r,z,\theta,t) = \frac{2}{\pi}\int^t g_\alpha(1)\ C_1 R_{PR}\ d\tau + \frac{2}{\pi}\int^t g_\beta(1)\ SV_1 R_{SR}\ d\tau + \frac{2}{\pi}\iint^t g_\alpha(2)\ C_1 R_{PR}\left(\frac{2}{pr}\right) d\tau\ dt + \frac{2}{\pi}\iint^t g_\beta(2)\ SV_1 R_{SR}\left(\frac{2}{pr}\right) d\tau\ dt + \frac{2}{\pi}\iint^t g_\beta(2)\ SH_1\left(\frac{-2}{r}\right) d\tau\ dt \qquad (24)$$

and

$$R_{PR} = -p\ , \qquad R_{SR} = \eta_\beta$$

for whole space and given by expression (18) for a receiver on a free surface. Similar expressions for the dip-slip result are obtained by changing the n to 1 and the factor in parentheses reduced by two.

The 45° dip-slip result is simply

$$Q_3(r,z,\theta,t) = \frac{2}{\pi}\int^t g_\alpha(1)\ C_3 R_{PR}\ dt = \frac{2}{\pi}\int^t g_\beta(1)\ SV_3 R_{PR}\ d\tau\ . \qquad (25)$$

Thus, to obtain the full solution requires 26 integrations for each time step which can be compared with numerical results obtained from closed form whole space solutions in spherical coordinates. Furthermore, the expressions in cylindrical coordinates are poorly behaved at small values of r, as we will see in the numerical results discussed in the next section.

NUMERICAL RESULTS

In this section we will present numerical evaluations based on the formalism presented earlier for models appropriate for shallow earthquakes. However, before these equations can be applied, we must specify the unknown function D(t), the slip history or the dislocation across the fault. Although there have been

many proposed slip histories, we will use the one suggested by Ohnaka [17] defined by

$$D(t) = \begin{cases} [1-(1+k_T t)\, e^{-k_T t}] & t > 0 \\ 0 & t < 0 \end{cases}$$

with the far field given by

$$\dot{D}(t) = k_T^2\, t\, e^{-k_T t}$$

because of its simplicity and its similarity to the Brune [18] far-field source. The artibrary constant k_T will be set at 1 and 10 to simulate a relatively large earthquake, M > 7, and a moderate size, M < 6. We assumed the seismic moment to be

$$M_o = 4\pi\rho_o \times 10^{23} = 3.4 \times 10^{24} \text{ ergs}$$

which is appropriate for the smaller event and the amplitudes will be expressed in cm. For earth models, we chose a whole space, a half space, and a layer over a half space, to keep the complexity at a minimum but still test some commonly held assumptions, see Table 1. That is, a number of authors have modeled local earthquakes by reducing the amplitudes of these observations by two and assuming that the Earth is a whole space, see for example, Trifunac [19].

As mentioned earlier, the expressions in cylindrical coordinates become unstable at small r's, since the near-field P wave response grows rapidly and is mostly cancelled by the SV wave. This means the numerical answer is the difference of large numbers, an unpleasant situation. For this reason, and to test the

TABLE 1

Model Parameters

Layer	Thickness km	P-Velocity km/s	S-Velocity km/s	Density g/cm^3
1	2.0	4.5	2.8	2.6
2	8.0	6.2	3.5	2.7

heavy algebra, we computed the whole space response in two ways. First, by evaluating the solution in spherical coordinates, given by Harkrider [7], and rotating the vectors into the directions r, z, and θ. The results are given on the right of Figure 2, with the corresponding solution in cylindrical coordinates, expressions (20), (22), and (24), given on the left. The short period results are identical, but the larger periods are somewhat off. Similar synthetics at larger ranges, Δ = 16 and 32 km, are identical for the short and long periods, since the near-field blow up is not so severe.

In Figure 3 we display the tangential results, V, for the whole space on the right, half space in the middle, and the asymptotic on the left. As might be expected, the comparison between the whole space and half space is quite good using the factor of two adjustment, although there is some distortion caused by the Rayleigh pole. On the other hand, the asymptotic solution is

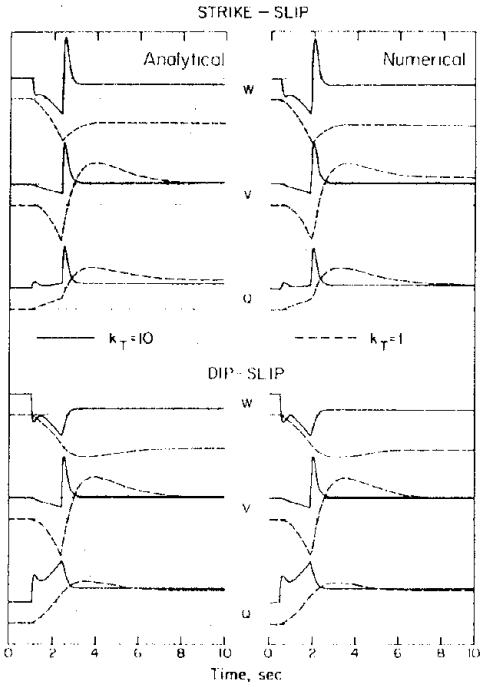

FIGURE 2. Comparison of the Whole Space Numerical Results (Cagniard-deHoop) with the Analytical Results. The Model Parameters are Specified by the Half-Space Given in Table 1 with the Top Layer Removed. The Amplitudes along Each Row are the Same and Given Explicitly in Figures 3, 4, and 5

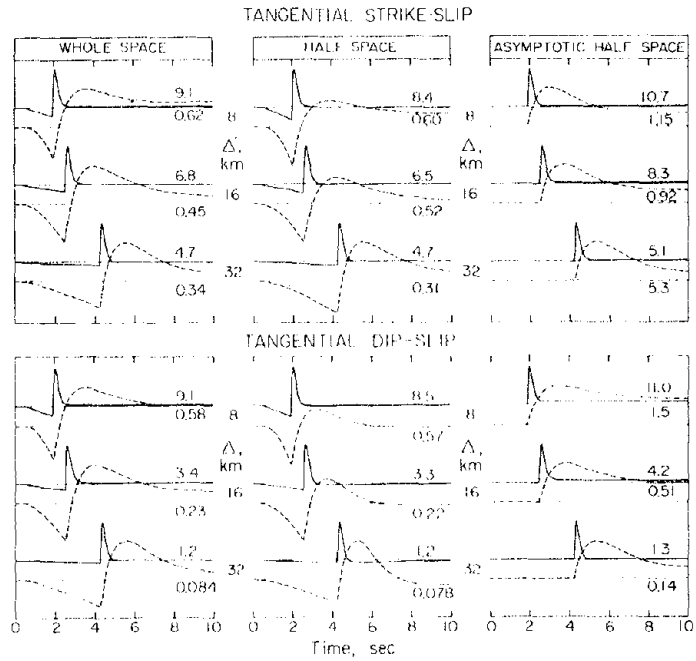

FIGURE 3. Comparison of the Full Cagniard Tangential Response Displayed on the Left and Middle with the Asymptotic Results on the Right. The Peak Amplitude in cm is Given for each Trace with the Whole Space Results Doubled. Model Parameters are Specified by the Half-Space in Table 1 with the Top Layer Removed

adequate at the largest range for the short periods, since most instruments would not detect the long period precursor. The only significant difference between the strike-slip and the dip-slip results is caused by the radiation pattern.

The corresponding comparisons for the vertical and radial components are given in Figures 4 and 5. For these components the factor of two, free surface adjustment, is adequate at $\Delta = 8$, but at larger ranges the diffracted P complicates the situation. On the other hand, the comparison between the full and asymptotic solutions is quite good for the short periods and even the long periods, except for the strike-slip radial components at $\Delta = 8$, 16 km. The reason for this is given by the strong near-field dependence for this particular component as can be seen from expression (24). The results for the 45° dip-slip case are similar to those in Figure 5 with the comparison between asymptotic and

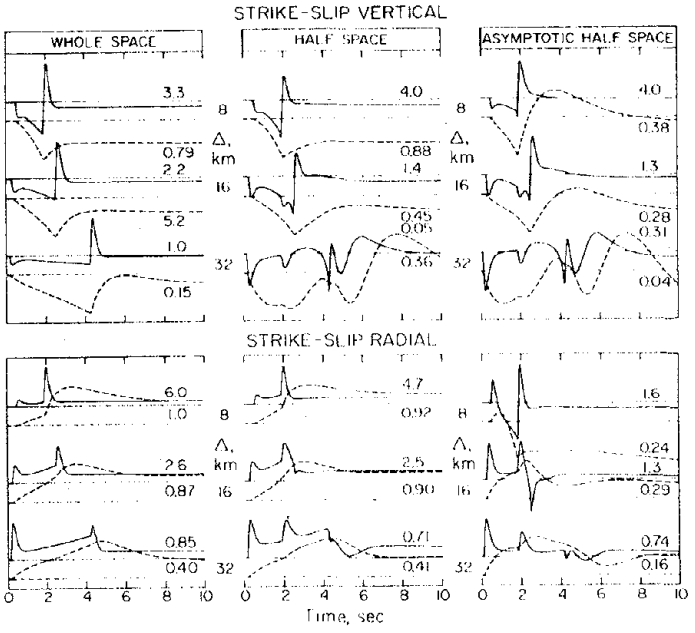

FIGURE 4. Vertical and Radial Comparisons for the Strike-Slip Orientation

exact being slightly better because of the smaller order number of the Bessel functions.

Actually, it is somewhat fortuitous that the asymptotic solution performs as well as it does, in that the full evaluation of the far-field term gives a poorer approximation to the full solution. The reason is that the so-called far-field term contains near-field information due to the unnatural (r) expansion. Thus, the far-field term grows rapidly in time, only to be partially cancelled by the explicit near-field term of another wave type.

The comparison between the asymptotic solution and the exact can be greatly improved at the larger ranges by including higher order terms, for example, see Figure 6. This solution does quite well already at r = 16 km, with the results for other orientations being nearly identical with the exact after summing two terms. On the other hand, the short period results at r = 8 km for the strike-slip case are better than those presented in Figure 4, but the longer period results are not. This is the normal behavior of asymptotic solutions, but in this situation the convergence criterion is complicated by the cancellations

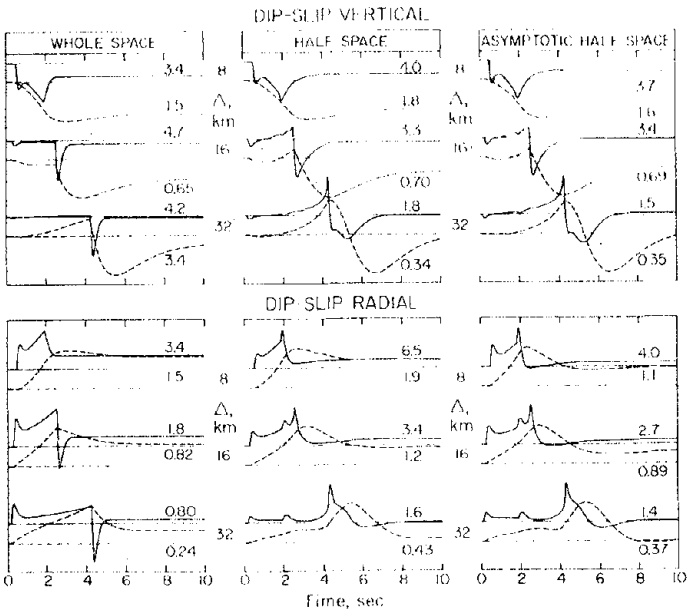

FIGURE 5. Vertical and Radial Comparisons for the Dip-Slip Orientation

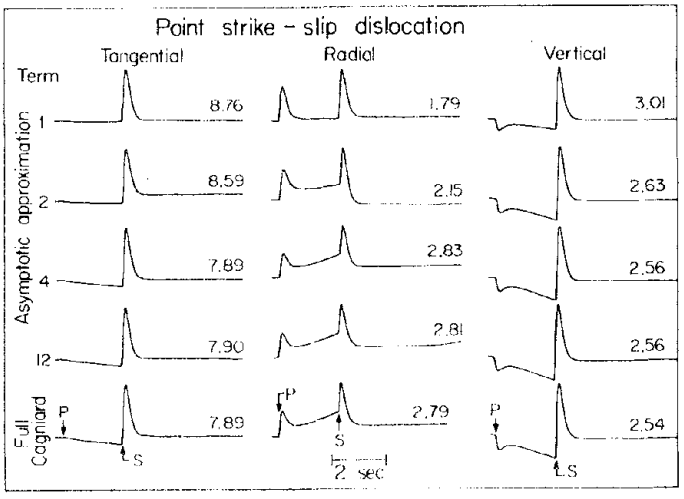

FIGURE 6. Comparison of the Various Components of Motion for a Strike-Slip Orientation at Δ = 16 km for a Whole Space. The Top Four Rows Contain the Asymptotic Summation after 1, 2, 4, and 12 Terms. The Full Solution is Displayed on the Bottom.

between the various wave types as mentioned earlier.

The general agreement between the full and asymptotic solution that occurs in Figures 4 and 5 also carries over into the layered model as displayed in Figure 7. The full Cagniard solution was generated by adding up rays where the integration process must be performed on each ray separately. Thus, the computation time is much longer than for the asymptotic solution which sums the rays before performing the convolution.

Fortunately, we generally do not need many rays at small ranges because the internal reflections are also small and the exact formalism can be applied. At larger ranges, where many rays are required to model the waveguide effects, we can use the asymptotic formulation.

An example application of the above asymptotic technique to earthquake modeling is given in Figure 8. The observed displacement is from a strike-slip earthquake of magnitude 5 occurring in the Imperial Valley, California. This event was located in a region of known velocity structure given at the top of the figure. The only unknown parameters were the source depth and

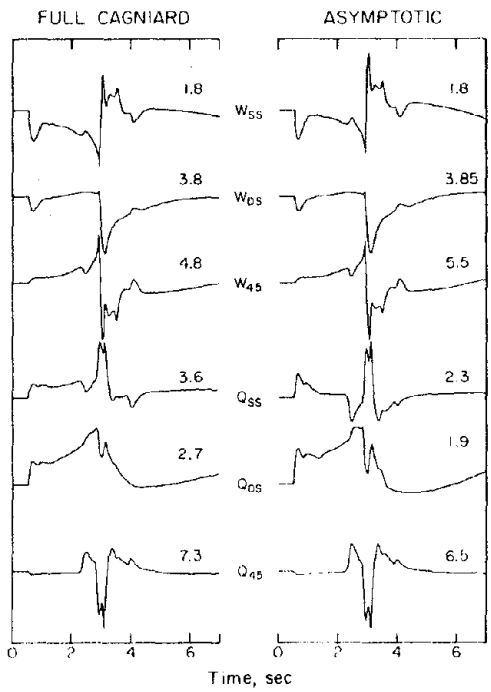

FIGURE 7. Comparison of the Full Solution with the Asymptotic Results (first term only) for a Layer over a Half-Space Model Given in Table 1.

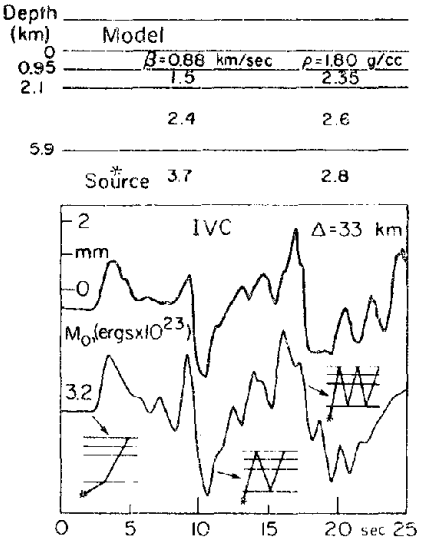

FIGURE 8. Comparison of a Synthetic with a Strong Motion Recording, IVC, of an Earthquake Occurring at Brawley, California, in November 1976. The Model Parameters Expressing the Known Structure are Given at the Top of the Figure with the Source at a Depth of 6.9 km. The Three Most Important Rays are Indicated Schematically.

slip history, D(t), assuming the source can be simulated by a point. After a diligent search the source depth of 6.9 km and a $\dot{D}(t)$ specified by a triangular pulse with duration 1.5 seconds was found to give the best fit, see Heaton and Helmberger [21] for details and a discussion of the other components. A similar study was conducted on a larger earthquake, the Borrego Mountain event, where the fault was replaced by a distribution of shear dislocations (Heaton and Helmberger [20]). Both of these studies involved observations at considerable distances, 30 and 60 km, respectively, where the first term of the asymptotic solution was assumed appropriate. However, because of the large numbers of strong-motion instruments presently being deployed, we will probably obtain close-in observations of a large earthquake in the near future, and thus the usefulness of the modeling procedure presented.

ACKNOWLEDGMENTS

This research was supported by the Earth Sciences Section, National Science Foundation Grant No. ENV76-10506 and by the

Advanced Research Projects Agency of the Department of Defense and was monitored by the Air Force Office of Scientific Research under Contract No. F49620-77-C-0022.

REFERENCES

1. D. L. Pekeris, Proc. Natl. Acad. Sci. U.S. 26, 433 (1940).
2. A. Ben-Menahem and M. Vered, Bull. Seism. Soc. Am. 63, 1611 (1973).
3. I. Kawasaki, Y. Suzuki, and R. Sato, J. Phys. Earth 21, 251 (1973).
4. H. Lamb, Phil. Trans. Roy. Soc. London A 203, 1 (1904).
5. N. A. Haskell, Bull. Seism. Soc. Am. 54, 1811 (1964).
6. A. T. de Hoop, "Representation theorems for the displacement in an elastic solid and their application to elastodynamic diffraction theory", Thesis, Techrische Hogeschool, Delft (1958).
7. D. G. Harkrider, Geophys. J. 47, 97 (1976).
8. D. V. Helmberger, Bull. Seism. Soc. Am. 64, 45 (1974).
9. C. A. Langston and D. V. Helmberger, Geophys. J. Roy. Astr. Soc. 42, 117 (1975).
10. F. J. Gilbert and D. V. Helmberger, Geophys. J. 27, 57 (1972).
11. D. G. Harkrider and D. V. Helmberger, Bull. Seism. Soc. Am. (in press, 1978).
12. A. T. de Hoop, Appl. Sci. Res. B 8, 349 (1960).
13. D. V. Helmberger, Bull. Seism. Soc. Am. 58, 179 (1968).
14. T. Spencer, Geophys. 25, 625 (1960).
15. D. V. Helmberger and S. D. Malone, J. Geophys. Res. 80, 4881 (1975).
16. L. Knopoff, R. W. Fredricks, A. F. Gangi, and L. P. Porter, Geophys. 22, 842 (1957).
17. M. Ohnaka, J. Phys. Earth 21, 39 (1973).
18. J. N. Brune, J. Geophys. Res. 75, 4997 (1970).
19. M. D. Trifunac, Bull. Seism. Soc. Am. 64, 149 (1974).
20. T. H. Heaton and D. V. Helmberger, Bull. Seism. Soc. Am. 67, 315 (1977).

21. T. H. Heaton and D. V. Helmberger, Bull. Seism. Soc. Am. (in press, 1978).

UNCLASSIFIED
SECURITY CLASSIFICATION OF THIS PAGE *(When Data Entered)*

REPORT DOCUMENTATION PAGE

READ INSTRUCTIONS BEFORE COMPLETING FORM

1. REPORT NUMBER: **AFOSR-TR-80-0641**	2. GOVT ACCESSION NO.: AD-A088 978
3. RECIPIENT'S CATALOG NUMBER:	
4. TITLE *(and Subtitle)*: MODELING EARTHQUAKES WITH GENERALIZED RAY THEORY	5. TYPE OF REPORT & PERIOD COVERED: Interim
	6. PERFORMING ORG. REPORT NUMBER:
7. AUTHOR(s): Donald V. Helmberger and David G. Harkrider	8. CONTRACT OR GRANT NUMBER(s): F49620-77-C-0022
9. PERFORMING ORGANIZATION NAME AND ADDRESS: California Institute of Technology, Seismological Laboratory, Pasadena, California 91125	10. PROGRAM ELEMENT, PROJECT, TASK AREA & WORK UNIT NUMBERS: 3291 62701E 8F10
11. CONTROLLING OFFICE NAME AND ADDRESS: Advanced Research Projects Agency/NMR, 1400 Wilson Boulevard, Arlington, Virginia 22209	12. REPORT DATE: 1978
	13. NUMBER OF PAGES: 20
14. MONITORING AGENCY NAME & ADDRESS *(if different from Controlling Office)*: Air Force Office of Scientific Research/NP, 1400 Wilson Boulevard, Arlington, Virginia 22209	15. SECURITY CLASS. *(of this report)*: Unclassified
	15a. DECLASSIFICATION/DOWNGRADING SCHEDULE:

16. DISTRIBUTION STATEMENT *(of this Report)*

Approved for public release; distribution unlimited.

17. DISTRIBUTION STATEMENT *(of the abstract entered in Block 20, if different from Report)*

B

18. SUPPLEMENTARY NOTES

Modern Problems in Elastic Wave Propagation pp499-518 , 1978

19. KEY WORDS *(Continue on reverse side if necessary and identify by block number)*

Source mechanisms, structural modeling.

20. ABSTRACT *(Continue on reverse side if necessary and identify by block number)*

The complete linear response of plane, elastic layered solid to a shear dislocation is investigated. The solution is expressed as a summation of generalized rays of the P, SV, and SH potentials. This allows the transient response to be obtained upon application of the Cagniard-deHoop technique. Numerical results of the full solution containing the near and far field terms are compared for a whole space, half space, and layered model with asymptotic solutions to establish the advantages and limitations of approximate methods.

DD FORM 1 JAN 73 1473 EDITION OF 1 NOV 65 IS OBSOLETE

UNCLASSIFIED